Article

Symmetric image registration with directly calculated inverse deformation field

Papiez, Bartek and Matuszewski, Bogdan

Annals of the BMVA Vol. 2012, No. 6, pp 1–14 (2012)

Symmetric image registration with directly calculated inverse deformation field

Bartlomiej W. Papież[1] and Bogdan J. Matuszewski

Applied Digital Signal and Image Processing Research Centre,
University of Central Lancashire, UK
⟨{bwpapiez, bmatuszewski1}@uclan.ac.uk⟩

Abstract

This paper presents a novel technique for a symmetric deformable image registration based on a new method for fast and accurate direct inversion of a large motion model deformation field. The proposed image registration algorithm maintain a one-to-one mapping between registered images by symmetrically warping them to each other, and by ensuring the inverse consistency criterion at each iteration. This makes the final estimation of forward and backward deformation fields anatomically plausible. The quantitative validation of the method has been performed on magnetic resonance data obtained for a pelvis area demonstrating applicability of the method to adaptive prostate radiotherapy. The experiments demonstrate the improved robustness in terms of inverse consistency error when compared to previously proposed methods for symmetric image registration.

1 Introduction

Image registration is a fundamental task in medical image processing aiming at an estimation of spatial transformation aligning two or more images that is in some sense optimal. As the image registration is an ill-posed problem it needs to be regularised by introducing additional *a priori* information to the estimation process [Matuszewski et al., 2006]. In the classical formulation of a non-parametric image registration, methods based on elastic, fluid, diffusive deformable models [Modersitzki, 2009] are commonly used to enforce a globally smooth dense deformation field. Although those methods have been shown to be fast and accurate, they have a drawback when used in clinical applications as they do not explicitly preserve organs' topology. To maintain the neighbourhood relationship and avoid anatomically incorrect deformations, the inverse consistency criterion has been introduced. In the early work on minimising the inverse consistency error (*ICE*), Christensen and Johnson [2001] proposed an algorithm jointly estimating a forward and a backward transformation. A similar idea of simultaneously reducing the ambiguous correspondence between

Annals of the BMVA Vol. 2012, No. 6, pp 1–14 (2012)

the forward and the backward transformation established via a variational framework and not limited to mono-modal images was presented in [Zhang et al., 2006].

Recently a diffeomorphic formulation of the image registration was proposed via flow in a suitable infinite-dimensional group of smooth, invertible transformations [Chefd'hotel et al., 2002], or via an approximation of a Lie group by a time-independent flow (stationary velocity field) [Arsigny et al., 2006]. The practical advances of this exponential mapping were incorporated into image registration frameworks e.g. for exponential updates of the deformation field [Vercauteren et al., 2009], by a single flow estimation [Ashburner, 2007], or a fully consistent Log-Domain approach [Vercauteren et al., 2008] as an efficient way of preventing transformation folding. All of these methods have been validated on MRI or CT images of a brain with relatively small deformations. Meanwhile the adaptive radiotherapy (ART) of prostate cancer must cope with significant changes of bladder and rectum shape and size. To overcome the problems related to effective and accurate large motion recovery, a symmetric warping between two images was introduced by registering these images to an intermediate image [Beg and Khan, 2007, Yang et al., 2008, Han et al., 2010, Papież and Matuszewski, 2011].

The main contributions of this paper are as follow. First, a new algorithm for estimation of the inverse deformation field is proposed, which can be seen as an extended version of the algorithm presented in [Christensen and Johnson, 2001]. Secondly, a novel method of image registration is proposed, utilising the previously mentioned method of inverse deformation field estimation for the symmetric image registration. The proposed method extends the approach presented in [Yang et al., 2008] by directly inverting the deformation field in each iteration. This allows the alleviation of constraints imposed on the maximum magnitude of the deformation field update in every iteration of the algorithm. Finally, an extensive comparison of the proposed registration scheme is conducted against two methods, namely: *small-step multiple pass approach* [Yang et al., 2008], which inspired this work, and the currently popular Log-Domain parameterised image registration with the implementation that was originally designed for the pelvic area data sets [Han et al., 2010]. All the aforementioned image registration methods take the advantage of the symmetric warping, so the results are comparable.

2 Symmetric image registration

The symmetric image registration is defined here for two input mono-modal images denoted by A and B. Corresponding deformation (displacement) fields at any spatial position are defined as: $\vec{x}$: $\vec{T}_{AC} = \vec{x} + \vec{u_f}(\vec{x})$ and $\vec{T}_{BC} = \vec{x} + \vec{u_b}(\vec{x})$ warping respectively image A and image B to an intermediate image C. Mathematically this can be stated as an optimisation problem:

$$\arg \min_{\vec{u_f},\vec{u_b}} \left(Sim(A \circ \vec{u_f}, B \circ \vec{u_b}) + \alpha_{u_f} Reg(\vec{u_f}) + \alpha_{u_b} Reg(\vec{u_b})\right) \tag{1}$$

where: Sim is a chosen similarity measure between images (e.g. the sum of squared differences [Modersitzki, 2009]), Reg is a regularisation term, and α_{u_f}, α_{u_b} are regularisation weights. The proposed method solves this problem by using the Demon-like force [Vercauteren et al., 2009] that is established in an iterative optimisation framework within the

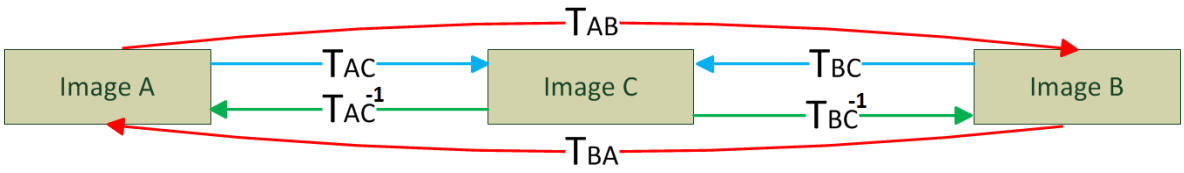

Figure 1: Symmetric image registration scheme

symmetric warping scheme [Yang et al., 2008]:

$$d\vec{u}^{\,i} = \frac{(A^i - B^i)(\nabla A^i + \nabla B^i)}{\|\nabla A^i + \nabla B^i\|^2 + (A^i - B^i)^2} \tag{2}$$

where: A^i and B^i represent warped images A and B, obtained by applying estimated deformation fields $\vec{u}_f^i$ and $\vec{u}_b^i$ respectively; ∇A^i and ∇B^i are gradients of images A^i and B^i; i is a current iteration index. In the Demon method the Gaussian smoothing is applied to the deformation and/or the update of the deformation field to regularise the solution rather than explicitly minimise *Reg* terms included in Equation 1.

The results of the symmetric registration towards the intermediate image C: $\vec{T}_{AC}$ and $\vec{T}_{BC}$ have to be inverted and the final transformations $\vec{T}_{AB}$ and $\vec{T}_{BA}$ are the compositions of $\vec{T}_{AC}$ and $\vec{T}_{BC}$ and their inverses $\vec{T}_{AC}^{-1}$ and $\vec{T}_{BC}^{-1}$: $\vec{T}_{AB} = \vec{T}_{BC}^{-1} \circ \vec{T}_{AC}$ and $\vec{T}_{BA} = \vec{T}_{AC}^{-1} \circ \vec{T}_{BC}$. The overall scheme of the symmetric image registration process is illustrated in Figure 1.

2.1 Small-step multiple pass approach

In the *small-step multiple pass approach* originally proposed in [Yang et al., 2008], it is assumed that:

$$\vec{u}_f^{\,i+1} = G_e * \left(\vec{u}_f^{\,i} \circ \left(G_f * \left(d\vec{u}^{\,i}\right)\right)\right) \quad \vec{u}_b^{\,i+1} = G_e * \left(\vec{u}_b^{\,i} \circ \left(G_f * \left(-d\vec{u}^{\,i}\right)\right)\right) \tag{3}$$

where: G_e* and G_f* represent Gaussian kernel convolutions which operate on updated displacement fields $\vec{u}_f$ and $\vec{u}_b$, and the update of the displacement field $\vec{du}$ respectively. This assumption simplifies significantly the estimation of the deformation fields but it holds only for small updates [Ashburner, 2007].

The Demon-like force does not guarantee the small-step update and therefore the explicit procedure of limiting the deformation magnitude is applied when the estimated update is greater than 0.4 voxel size (this limit was chosen ad hoc by Yang et al. [2008] following the limits that were determined for B-Spline deformable image registration [Rueckert et al., 2006]). However, image registration in the adaptive radiotherapy (ART) requires not only to be accurate but also fast and the update magnitude limiting procedure contradicts these requirements. Additionally, the quality of the approximation of the inverse update needs to be checked in practice.

2.2 Direct inverse deformation field approach

The direct inverse deformation field approach [Papież and Matuszewski, 2011] is built on the previous approach by directly inverting the update of the deformation field after each

iteration. The proposed update scheme is defined as follows:

$$\vec{u_f}^{\,i+1} = G_e * \left(\vec{u}_f^{\,i} \circ \left(G_f * \left(d\vec{u}^{\,i}\right)\right)\right) \quad \vec{u}_b^{\,i+1} = G_e * \left(\vec{u}_b^{\,i} \circ \left(G_f * \left(d\vec{u}^{\,i}\right)^{-1}\right)\right) \tag{4}$$

The scheme in Equation 4 in contrast to Equation 3 (compare formula for updating $\vec{u}_b^{\,i+1}$) uses the direct inverse update of the deformation which does not suffer from the limitations of the *small-step multiple pass approach* (that is because of $d\vec{u}^{\,i} \circ (d\vec{u}^{\,i})^{-1}(\vec{x}) = \vec{x}$).

In the *small-step multiple pass approach* and the direct inverse approach, there is a need to estimate the inverse deformation fields T_{AC} and T_{BC}. This has to be done accurately and fast especially for the direct inverse approach, where the inverse is also calculated in each iteration. In *small-step multiple pass approach*, the inverse transformations of $\vec{T}_{AC}$ and $\vec{T}_{BC}$ are calculated using the method proposed by Ashburner et al. [2000]. A new method is presented in this paper that is based on the method proposed by Christensen and Johnson [2001] but is more accurate and robust then previously reported methods.

2.2.1 Christensen's method

The procedure used to compute the inverse transformation proposed in [Christensen and Johnson, 2001] assumes that an input transformation $\vec{T}_f$ is a continuously differentiable mapping from $\Omega \to \Omega$ with a positive Jacobian determinant for all $\vec{x} \in \Omega$. An inverse deformation field can be found by selecting a point $\vec{y} \in \Omega$ and carrying out an iterative process to search for a point $\vec{x}$ which makes the distance $\|\vec{y} - \vec{T}_f(\vec{x})\|$ smaller than a desired threshold ξ. The iterations defining the inverse transformation are given by:

$$\vec{x}_{k+1} = \vec{x}_k + \frac{\vec{y} - \vec{T}_f(\vec{x}_k)}{2} \tag{5}$$

The initially selected point $\vec{x}_0$ should not be far from the final estimate $\vec{x}$. The drawback of this method is that the method is not established via a formal mathematical scheme. Although the method has been shown to converge to good results when the minimum value of the Jacobian determinant is greater than zero, the method has been validated for relatively small deformations fields (i.e. the CT and MRI brain scans [Christensen and Johnson, 2001], [Johnson and Christensen, 2002]).

2.2.2 Proposed deformation field inversion model

In the proposed method the inversion of the deformation field is achieved by using a Newton-Raphson like method. Let us define a point misalignment function $\vec{f}(\vec{x})$:

$$\vec{f}(\vec{x}) = \vec{y} - \vec{T}_f(\vec{x}) \tag{6}$$

For each $\vec{y} \in \Omega$, the aim is to find corresponding $\vec{x}$ which will make $\vec{f}(\vec{x})$ as close to zero as possible. This is achieved in an iterative fashion:

$$\vec{x}^{\,k+1} = \vec{x}^{\,k} + d\vec{x}^{\,k} \tag{7}$$

Approximating the misalignment function using first order Taylor series expansion:

$$\vec{f}(\vec{x} + d\vec{x}) \approx \vec{f}(\vec{x}) + J(\vec{f}(\vec{x}))d\vec{x} \tag{8}$$

where $J(\vec{f}(\vec{x}))$ denotes the Jacobian matrix, assuming $\vec{f}(\vec{x}+d\vec{x}) = 0$ and introducing regularisation, the updates $d\vec{x}^{\,k}$ can be calculated from a set of linear equations:

$$(J(\vec{f}(\vec{x})) + \beta I)d\vec{x} = -\vec{f}(\vec{x}) \tag{9}$$

where I is an n-dimensional diagonal matrix, and β is a position dependent regularisation parameter. The regularisation is introduced only for the areas where the determinant of $J(\vec{f}(\vec{x}))$ is close to zero.

2.3 Log-Domain parameterisation approach

Recently, a Log-Euclidean framework was proposed by Arsigny et al. [2006] to represent diffeomorphic transformation $\vec{T}$ using a stationary velocity field $\vec{v}$. Based on this framework the inverse consistent symmetric image registration has been proposed by Han et al. [2010], where the displacement fields $\vec{u}_f$ and $\vec{u}_b$ are calculated via corresponding velocity fields $\vec{v}_f$ and $\vec{v}_b$, that are parameterised using stationary velocity field $\vec{v}$:

$$\vec{v}_f^{\,i+1} = log(exp(\vec{v}^{\,i}) \circ exp(d\vec{v}^{\,i})) \quad \vec{v}_b^{\,i+1} = log(exp(-\vec{v}^{\,i}) \circ exp(-d\vec{v}^{\,i})) \tag{10}$$

where $\vec{dv}^{\,i}$ is defined in the same way as $\vec{du}^{\,i}$ in Equation 2. To maintain the inverse consistency criterion the velocity field $\vec{v}^{i+1}$ is calculated based on the average of the forward and backward update of transformations in Log-domain space as follows:

$$\vec{v}^{\,i+1} = \frac{1}{2} log(exp(\vec{v}_f^{\,i+1}) \circ exp(\vec{v}_b^{\,i+1})) \tag{11}$$

The principal logarithm of exponential mappings for Equation 10 and Equation 11 is approximated using the Baker-Campbell-Hausdorff (BCH) formula [Bossa et al., 2007, Vercauteren et al., 2008]. The advantage of this approach is that the final transformations $\vec{T}_{AB}$ and $\vec{T}_{BA}$ can be obtained by the composition of exponentiation of the velocity field $\vec{v}$:

$$\begin{aligned} \vec{T}_{AB} &= \vec{x} + exp(\vec{v}) \circ (exp(-\vec{v}))^{-1} = \vec{x} + exp(2\vec{v}) \\ \vec{T}_{BA} &= \vec{x} + exp(-\vec{v}) \circ (exp(\vec{v}))^{-1} = \vec{x} + exp(-2\vec{v}) \end{aligned} \tag{12}$$

Although the results presented in [Han et al., 2010, Vercauteren et al., 2008] show good performance, it has been shown also that computing the exponential mapping has some limitations for large deformations [Bossa et al., 2008].

3 Experimental results

The experimental section consists of two types of validation. First, the methods for inverting the deformation field are evaluated (in section 3.3). Then, in section 3.4 the quantitative evaluation of the introduced image registration algorithms namely *the small-step multi-pass approach*, direct inverse approach, and Log-Domain approach, is conducted to assess their accuracy and robustness.

Annals of the BMVA Vol. 2012, No. 6, pp 1–14 (2012)

3.1 Evaluation criteria

The algorithms for inverting the deformation field are compared with respect to the inverse consistency error (ICE) (see [Song et al., 2010] for the detailed description). The ICE is defined here as an average distance between the original point in one image and its position in this image after mapping to the another image and subsequent mapping back to the original image:

$$ICE = \frac{1}{2}(\|(\vec{x} - (\vec{T}_{AC} \circ \vec{T}_{AC}^{-1})(\vec{x}))\| + \|(\vec{x} - (\vec{T}_{AC}^{-1} \circ \vec{T}_{AC})(\vec{x}))\|) \tag{13}$$

The maximal ICE ($maxICE$) is also calculated:

$$maxICE = max(\|(\vec{x} - (\vec{T}_{AC} \circ \vec{T}_{AC}^{-1})(\vec{x}))\|, \|(\vec{x} - (\vec{T}_{AC}^{-1} \circ \vec{T}_{AC})(\vec{x}))\|) \tag{14}$$

The image registration quality is assessed by the commonly used criteria: the sum of squared differences (SSD) of the image intensities before and after registration, and the harmonic energy (HE) [Vercauteren et al., 2009] of the estimated deformation fields which reflects the smoothness of the deformation field. The ICE and the $maxICE$ as defined in Equations 13 and 14 are also used but this time with transformation $\vec{T}_{AC}$ replaced by $\vec{T}_{AB}$ and transformation $\vec{T}_{AC}^{-1}$ replaced respectively by $\vec{T}_{BA}$. The ICE criteria measure only the consistency between the forward and the backward transformation, while the accuracy of the transformation is not assessed. As the symmetric image registration is a case of group-wise registration when two images are registered the transitivity error (TE) and maximal TE ($maxTE$) [Song et al., 2010] are also calculated. The transitivity error measures the difference between the composition of deformation fields $\vec{T_{AC}} \circ \vec{T}_{CB}$ ($\vec{T_{BC}} \circ \vec{T}_{CA}$) and the corresponding target deformation field $\vec{T}_{AB}$ ($\vec{T}_{BA}$). The TE is defined as follows:

$$TE = \frac{1}{2}(\|(\vec{T}_{AC} \circ \vec{T}_{CB})(\vec{x}) - \vec{T}_{AB}(\vec{x})\| + \|(\vec{T}_{BC} \circ \vec{T}_{CA})(\vec{x}) - \vec{T}_{BA}(\vec{x})\|) \tag{15}$$

and maximal TE ($maxTE$):

$$maxTE = max(\|(\vec{T}_{AC} \circ \vec{T}_{CB})(\vec{x}) - \vec{T}_{AB}(\vec{x})\|, \|(\vec{T}_{BC} \circ \vec{T}_{CA})(\vec{x}) - \vec{T}_{BA}(\vec{x})\|). \tag{16}$$

The TE reflects the consistency of the composed deformation fields.

Moreover, the average of the relative overlap (RO) (also called the Tanimoto coefficient or the Jaccard index) between prostate P_A (P_B) segmented in the image A (B) and prostate $P_{A_{warp}}$ ($P_{B_{warp}}$) segmented in the warped image $A \circ \vec{T}_{AB}$ ($B \circ \vec{T}_{BA}$), was used to evaluate the registration performance in terms of the prostate position. The RO has been defined as:

$$RO = \frac{1}{2}\left(\frac{numberOfVoxels(P_A \cap P_{B_{warp}})}{numberOfVoxels(P_A \cup P_{B_{warp}})} + \frac{numberOfVoxels(P_B \cap P_{A_{warp}})}{numberOfVoxels(P_B \cup P_{A_{warp}})}\right) \tag{17}$$

Calculating the RO in the respective native spaces (space of image A (or image B)) rather than *half* space (space of image C) has been done in a spirit of a typical time-sequence analysis of pre- and per- treatment images [Castadot et al., 2008].

Annals of the BMVA Vol. 2012, No. 6, pp 1–14 (2012)

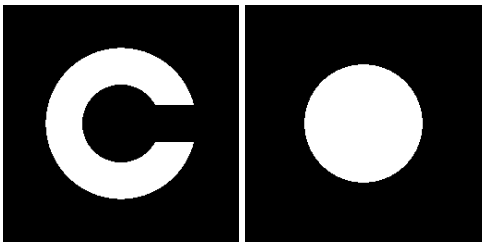

Figure 2: Synthetic images A (on the left) and B (on the right) used to generate a deformation field with large value of the Jacobian determinant.

3.2 Data sets description

3.2.1 Synthetic example

The synthetic data set consists of two 2D images (so-called *c to circle test example*) of size 256×256 pixels each shown in Figure 2. The significant deformation in terms of the determinant of $J(\vec{T}(\vec{x}))$ has to be estimated to achieve correct image registration results. The estimated deformation fields T_{AC} and T_{BC} are used to assess the accuracy of the methods for inverting the deformation field. The dispersion of 0.25 and 1.0 was used respectively for G_e and G_f smoothing Gaussian kernels; the image registration terminated when it reached the maximum of 50 iteration or the difference between estimated deformation fields in the current and previous iteration fell below a selected value [Chefd'hotel et al., 2002]. The bilinear interpolation method was implemented to calculate image and deformation field values on non-grid positions.

3.2.2 Real data example

The data set used in these experiments consists of 5 MRI volumes of $320 \times 240 \times 30$ voxels with voxel size of $1.0 \times 1.0 \times 3.0\text{mm}^3$. In each scan, the data exhibit significant changes of bladder size and shape. A sample of the data is shown in Figure 3. Since in symmetric image registration both input images are warped and therefore there is no so-called reference image, all images are used to support full fold-over cross validation. Registration described as *Set 1-5* means that *Image 1* and *Image 5* were used for evaluation. The dispersion of 0.5 and 1.0 was used for G_e and G_f smoothing Gaussian kernels respectively for all tested methods, the trilinear interpolation, and the same termination criterion as used for the synthetic data.

3.3 Validation of the inverse deformation field estimation

Validation of the inverse deformation field estimation methods is conducted using the spatial deformation field calculated during the symmetric image registration. The results of this registration towards the intermediate image C: T_{AC} and T_{BC} are used as input deformation fields for the methods that are inverting deformation field. Example of this input deformation is shown in Figure 4a. In the experiments, the Christensen's (section 2.2.1, [Christensen and Johnson, 2001]), the proposed (section 2.2.2), and Ashburner's [Ashburner et al., 2000] method were tested. For the Christensen's and the proposed method the iterations are terminated when they reach either the maximum iterations number of 1000 or the desired distance

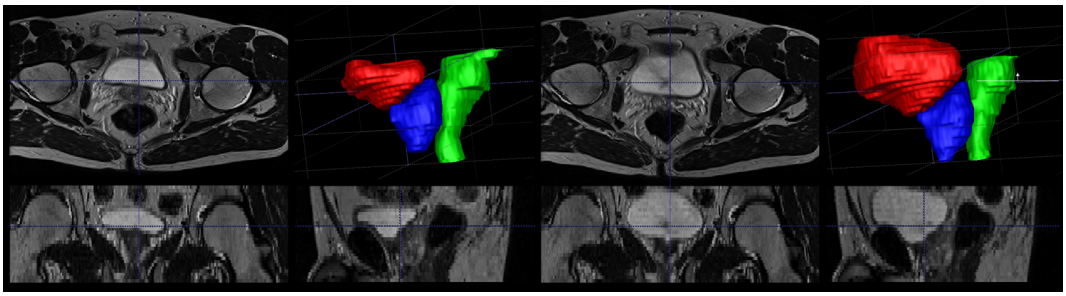

Figure 3: Example of the real data used in the experiments: volume labelled as *Image 1* (left) and volume labelled as *Image 5* (right). Segmented bladder, rectum and prostate are shown in red, green and blue respectively.

threshold value of 0.001. For the proposed method, parameter β (in Equation 9) was chosen to make the minimum value of $det(J(\vec{f}(\vec{x})))$ greater than 0.1. For the Ashburner's method [Ashburner et al., 2000], the implementation from the SPM library [Friston et al., 2007] was used in the experiments.

	Inverse consistency error			
		T_{AC} *and* T_{AC}^{-1}		*max*
	Christensen	Ashburner	proposed method	$det(J)$
(2D) Fig. 2	0.210 (38.5)	-	0.158 (28.9)	2.1
(3D) Set 2	0.015 (0.65)	0.134 (4.67)	0.015 (0.65)	4.9
(3D) Set 3	0.016 (0.52)	0.150 (3.75)	0.015 (0.51)	5.9
(3D) Set 4	0.017 (2.56)	0.186 (5.45)	0.016 (0.76)	8.4
(3D) Set 5	0.021 (6.64)	0.261 (12.0)	0.020 (1.11)	12.0
		T_{BC} *and* T_{BC}^{-1}		*max*
	Christensen	Ashburner	proposed method	$det(J)$
(2D) Fig. 2	0.736 (49.0)	-	0.004 (0.89)	14.9
(3D) Set 2	0.015 (0.49)	0.131 (4.76)	0.015 (0.49)	4.7
(3D) Set 3	0.016 (0.83)	0.147 (5.78)	0.016 (0.83)	4.3
(3D) Set 4	0.017 (1.10)	0.197 (10.3)	0.017 (1.09)	5.5
(3D) Set 5	0.021 (3.62)	0.296 (16.4)	0.021 (1.67)	8.0

Table 1: Comparison results for inverse deformation field estimation algorithms. The mean of ICE, maximum of $maxICE$ (in brackets), and maximum of $det(J)$ are shown for each algorithm and each test data. Both 2D synthetic data and real 3D MRI data, showing pelvic region, were used in the experiments.

For the synthetic data, Figure 4 shows that the inverse deformation field produced by the proposed method (Figure 4f) is much smoother than that produced by the Christensen's method (Figure 4b), especially in the area where the Jacobian determinant has large values (Figure 4e). In terms of the ICE values shown in Figure 4c-d,g-h, although both methods have the maximum ICE value around the middle of the image, the ICE maximum value produced by the Christensen's method is significantly higher. Furthermore, the mean value

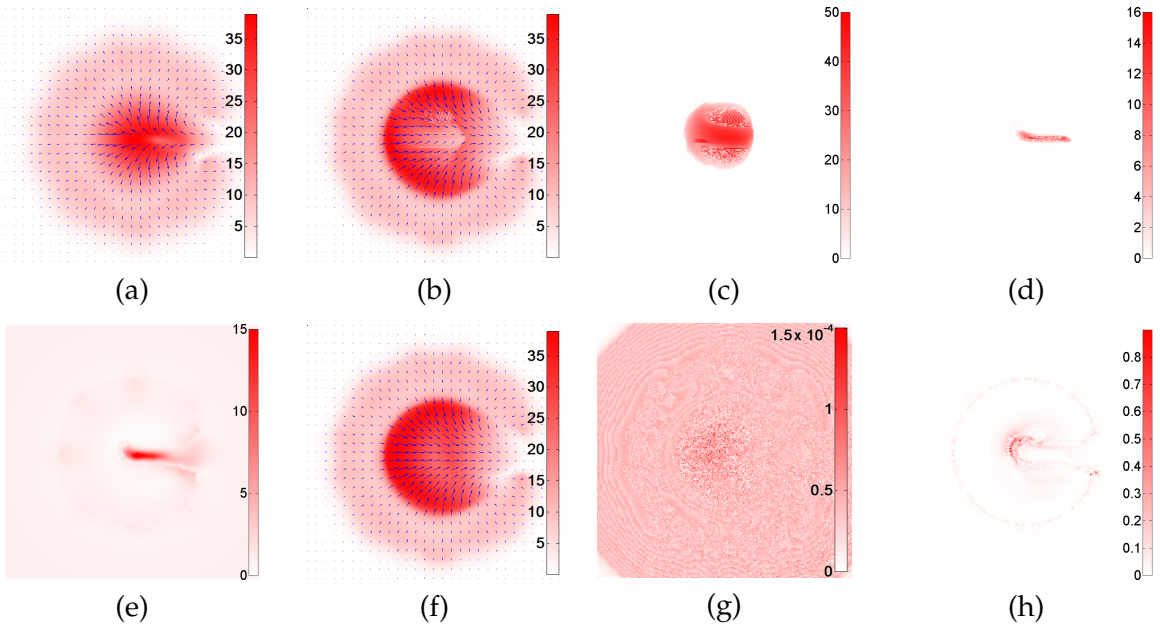

Figure 4: Results for the synthetic data shown in Figure 2: (a) input deformation field T_{BC}, (b) inverse deformation field estimated using [Christensen and Johnson, 2001], (c) $ICE_{\vec{T}_{BC},\vec{T}_{BC}^{-1}}$ and (d) $ICE_{\vec{T}_{BC}^{-1},\vec{T}_{BC}}$ using [Christensen and Johnson, 2001], (e) point wise calculated Jacobian determinant of the input transformation T_{BC}, (f) inverse deformation field estimated using the proposed method, (g) $ICE_{\vec{T}_{BC},\vec{T}_{BC}^{-1}}$ and (h) $ICE_{\vec{T}_{BC}^{-1},\vec{T}_{BC}}$ using the proposed method, where e.g. $ICE_{\vec{T}_{BC},\vec{T}_{BC}^{-1}}$ represents one sided inverse consistency error defined as: $ICE_{\vec{T}_{BC},\vec{T}_{BC}^{-1}} = \|(\vec{x} - (\vec{T}_{BC} \circ \vec{T}_{BC}^{-1})(\vec{x}))\|$

of ICE and the maximum value of $maxICE$, both calculated from all the pixel locations, computed based on $\vec{T}_{AC}/\vec{T}_{AC}^{-1}$, and on $\vec{T}_{BC}/\vec{T}_{BC}^{-1}$ are also listed in the corresponding first rows of Table 1, where both the mean ICE and maximum $maxICE$ values for the Christensen's method are seen to be higher.

For the MRI volumetric images, the data set consist of five volumes, and image registration was performed with respect to the first volume. The mean ICE and the maximum of $maxICE$ values produced by the two commonly used methods [Christensen and Johnson, 2001, Ashburner et al., 2000] and the proposed method are given in Table 1. From Table 1, it can be seen that the maximum value of the Jacobian determinant is increasing from set 2 to set 5 which correspond to increasing organ shape changes between the images. In terms of performance, Ashburner's method is seen to be the worst with highest mean ICE and maximum $maxICE$ values. The proposed method can be seen to be the best. Whereas it has comparable mean ICE and maximum $maxICE$ values to those obtained from Christensen's method for small organ shape deformation, it performs better than Christensen's method for the larger organ shape deformations.

One iteration of the proposed method of inverting the deformation field is computationally more expensive when compared to the Christensen's method due to additional calculation for solving system of linear equations (Equation 9). However, an additional cost can be justified in general either by more accurate results achieved using this method, or in some

cases by a fewer number of executed iterations to reach a similar solution.

3.4 Comparison of symmetric image registration algorithms

The results presented in Table 2 show that all the registration methods presented in the previous section perform similarly in terms of the sum of squared differences. The proposed method as well as *small-step multiple pass approach* produce higher values of the harmonic energy of transformations than the Log-Domain approach. This confirms the results for smoothness assessment of deformation field for the Log-domain parametrisation from [Vercauteren et al., 2008].

The results presented in Table 3 show that the *small-step approach* produce the highest ICE and $maxICE$ especially when a significant deformation needs to estimated (e.g. *Set 1-4* and *Set 1-5*), while for the Log-domain and the proposed method the corresponding ICE are significantly lower. When the $maxICE$ is compared, the proposed method produces slightly lower errors. This shows that both method the Log-domain approach and the proposed method enforce the inverse consistency criterion during the registration. Although the transitivity error for all methods is similar, the proposed method is the most accurate, and less sensitive to the magnitude of the deformations as seen in Table 4.

Finally, all compared methods produce similar results in terms of the prostate relative overlap (RO) as presented in Table 5. This suggests that the numerical improvements in terms of ICE ($maxICE$) and TE ($maxTE$) have a minor impact on the prostate RO. This can be explained by the fact that the image registration for that particular region is driven mostly by the adjacent organs with the higher intensity contrast (such as bladder and rectum). Although all methods show a similar RO values, it is noteworthy that transformations with lower ICE can indicate physically more plausible deformations, which make a difference in treatment planning (e.g. during dose painting).

	Quality of registration						
	before	*small step*		Log-Domain		proposed method	
	SSD	SSD	HE	SSD	HE	SSD	HE
(3D) Set 1-2	6.0	0.6	0.07	0.6	0.05	0.6	0.10
(3D) Set 1-3	7.5	0.8	0.07	0.8	0.06	0.8	0.11
(3D) Set 1-4	9.4	1.0	0.09	1.1	0.08	0.9	0.11
(3D) Set 1-5	9.1	1.2	0.15	1.3	0.13	1.2	0.15
(3D) Set 2-3	2.2	0.6	0.06	0.6	0.05	0.6	0.07
(3D) Set 2-4	4.5	0.8	0.08	0.8	0.06	0.8	0.08
(3D) Set 2-5	6.2	1.3	0.17	1.4	0.14	1.3	0.20
(3D) Set 3-4	2.5	0.5	0.06	0.5	0.05	0.5	0.07
(3D) Set 3-5	4.5	1.0	0.12	1.0	0.09	1.0	0.11
(3D) Set 4-5	2.7	0.9	0.11	0.9	0.09	0.9	0.11
Average	5.46	0.87	0.098	0.90	0.080	0.86	0.111

Table 2: Comparison results for image registration algorithms using sum of squared differences (SSD) before and after registration, and the harmonic energy (HE). The results have been obtained for the real MRI volume data set of pelvic region (corresponding data samples are shown in Figure 3).

	Inverse consistency error for T_{AB} and T_{AB}^{-1}		
	small step	Log-Domain	proposed method
(3D) Set 1-2	0.26 (3.82)	0.05 (3.57)	0.04 (3.17)
(3D) Set 1-3	0.29 (5.54)	0.05 (4.87)	0.05 (3.57)
(3D) Set 1-4	0.40 (10.4)	0.07 (6.59)	0.06 (4.72)
(3D) Set 1-5	0.58 (16.6)	0.09 (8.17)	0.08 (8.15)
(3D) Set 2-3	0.14 (4.60)	0.05 (3.93)	0.04 (3.57)
(3D) Set 2-4	0.22 (7.25)	0.06 (5.42)	0.05 (3.55)
(3D) Set 2-5	0.49 (13.2)	0.09 (5.65)	0.09 (4.18)
(3D) Set 3-4	0.17 (4.81)	0.04 (3.13)	0.04 (2.81)
(3D) Set 3-5	0.35 (10.2)	0.07 (5.28)	0.07 (4.77)
(3D) Set 4-5	0.30 (9.08)	0.07 (5.15)	0.06 (5.91)
Average	0.32 (8.55)	0.064 (5.18)	0.057 (4.44)

Table 3: Comparison results for image registration algorithms using the mean of ICE, and the maximum of $maxICE$ (in brackets).

4 Conclusions

Registration of pelvic area images is challenging due to possible significant shape and size changes of bladder and rectum. To provide an accurate method for estimation of the prostate position, the symmetric image registration framework based on the direct inversion of the deformation field has been proposed in this paper. Additionally a new method for estimation of the inverse deformation field has also been suggested.

The proposed method for inverting deformation field can be seen as an extension of the method proposed by Christensen and Johnson [2001]. Using the maximum value of the Jacobian determinant, $max(det(J))$, as an indicator of the level of the deformation, the performance of the Christensen's method is seen to deteriorate strongly with $max(det(J))$ exceeding 6, whereas the proposed method is able to handle large deformation with $max(det(J))$ significantly greater than 6 as shown in Tab. 1.

Furthermore, in the symmetric deformable image registration framework, the proposed method can replace *the small-step multiple pass* approach in each iteration step and offer the advantage of higher accuracy by removing the magnitude limiting procedure. The quantitative validation performed on real MRI and synthetic data shows that the proposed modifications results in the reduction of the inverse consistency and transitivity error measures when compared with *the small-step multiple pass* algorithm with the Wilcoxon rank test p value of 0.0002 (0.0072) and 0.002 (0.001) for the mean ICE (maximum $maxICE$) and mean TE (maximum $maxTE$) respectively. When compared with the Log-domain approach the proposed method produces similar results in terms of inverse consistency error measure and is lower in terms of transitivity error measures with the Wilcoxon rank test p value of 0.0007 for $meanTE$ and 0.06 for maximum $maxTE$.

Acknowledgement

This work was supported by the Engineering and Physical Sciences Research Council [grant number EP/D077540/1].

	Transitivity error for T_{AB} *and* T_{AB}^{-1}		
	small step	Log-Domain	proposed method
(3D) Set 1-2	0.003 (1.76)	0.003 (0.86)	10^{-4} (0.84)
(3D) Set 1-3	0.004 (2.16)	0.004 (1.22)	0.001 (1.16)
(3D) Set 1-4	0.005 (1.96)	0.005 (2.19)	0.001 (1.01)
(3D) Set 1-5	0.008 (2.76)	0.011 (4.22)	0.002 (1.03)
(3D) Set 2-3	0.003 (1.46)	0.002 (1.24)	10^{-4} (1.27)
(3D) Set 2-4	0.004 (1.84)	0.004 (1.62)	10^{-4} (0.77)
(3D) Set 2-5	0.011 (2.61)	0.011 (4.21)	0.003 (1.53)
(3D) Set 3-4	0.003 (1.32)	0.002 (0.79)	10^{-4} (0.86)
(3D) Set 3-5	0.007 (3.42)	0.007 (3.29)	0.002 (1.51)
(3D) Set 4-5	0.005 (2.54)	0.005 (1.73)	0.002 (1.61)
Average	0.005 (2.18)	0.005 (2.13)	0.001 (1.16)

Table 4: Comparison results for image registration algorithms using the mean of TE, and the maximum $maxTE$ (in brackets).

References

V. Arsigny, O. Commowick, X. Pennec, and N. Ayache. A log-euclidean framework for statistics on diffeomorphisms. In *Proc. 13th Int. Conference on Medical Image Computing and Computer-Assisted Intervention*, pages 924–931. Springer, 2006.

J. Ashburner. A fast diffeomorphic image registration algorithm. *NeuroImage*, 38(1):95–113, 2007.

J. Ashburner, J. Andersson, and K.J. Friston. Image registration using a symmetric prior - in three-dimensions. *Human Brain Mapping*, 9(4):212–225, 2000.

M. F. Beg and A. Khan. Symmetric data attachment terms for large deformation image registration. *IEEE Trans. on Medical Imaging*, 26(9):1179–1189, 2007.

M. Bossa, M. Hernandez, and S. Olmos. Contributions to 3d diffeomorphic atlas estimation: application to brain images. In *Proc. 10th Medical Image Computing and Computer-Assisted Intervention*, pages 667–674. Springer, 2007.

M. Bossa, E. Zacur, and S. Olmos. Algorithms for the group exponential of diffeomorphisms: performance evaluation. In *Proc. IEEE Computer Vision and Pattern Recognition Workshop on Mathematical Methods in Biomedical Image Analysis*, 2008.

P. Castadot, J.A Lee, A. Parraga, X. Geets, B. Macq, and V. Grégoire. Comparison of 12 deformable registration strategies in adaptive radiation therapy for the treatment of head and neck tumors. *Radiotherapy & Oncology*, 89:1–12, 2008.

C. Chefd'hotel, G. Hermosillo, and O. Faugeras. Flows of diffeomorphisms for multimodal image registration. In *Proc. IEEE Int. Symposium on Biomedical Imaging*, pages 753–756, 2002.

G.E. Christensen and H.J. Johnson. Consistent image registration. *IEEE Trans. on Medical Imaging*, 20(7):568–582, 2001.

	Prostate relative overlap			
	before	*small step*	Log-Domain	proposed method
(3D) Set 1-2	0.80	0.82	0.82	0.82
(3D) Set 1-3	0.81	0.82	0.83	0.82
(3D) Set 1-4	0.62	0.77	0.77	0.77
(3D) Set 1-5	0.54	0.74	0.75	0.75
(3D) Set 2-3	0.85	0.86	0.87	0.86
(3D) Set 2-4	0.66	0.80	0.80	0.80
(3D) Set 2-5	0.57	0.80	0.79	0.79
(3D) Set 3-4	0.69	0.82	0.82	0.82
(3D) Set 3-5	0.60	0.82	0.82	0.82
(3D) Set 4-5	0.77	0.79	0.79	0.80
Average	0.69	0.80	0.80	0.80

Table 5: Comparison results for image registration algorithms using prostate relative overlap criterion.

K.J. Friston, J. Ashburner, S.J. Kiebel, T.E. Nichols, and W.D. Penny. *Statistical Parametric Mapping: The Analysis of Functional Brain Images*. Academic Press, 2007.

X. Han, L.S. Hibbard, and V. Willcut. An efficient inverse-consistent diffeomorphic image registration method for prostate adaptive radiotherapy. In *Proc. MICCAI Int. Workshop on Prostate Cancer Imaging. Computer-Aided Diagnosis, Prognosis, and Intervention*, pages 34–41. Springer, 2010.

H. J. Johnson and G. E. Christensen. Consistent landmark and intensity-based image registration. *IEEE Trans. on Medical Imaging*, 21(5):450–461, 2002.

B.J. Matuszewski, J.K. Shen, L.K. Shark, and Moore C.J. Estimation of internal body deformations using an elastic registration technique. In *Proc. Int. Conference on Medical Information Visualisation - BioMedical Visualisation*, pages 15–20, 2006.

J. Modersitzki. *FAIR: Flexible Algorithms for Image Registration*. SIAM, Philadelphia, 2009.

B.W. Papież and B.J. Matuszewski. Direct inverse deformation field approach to pelvic-area symmetric image registration. In *Proc. Conference on Medical Image Understanding and Analysis*, pages 193–197, 2011.

D. Rueckert, P. Aljabar, R.A. Heckemann, J.V. Hajnal, and A. Hammers. Diffeomorphic registration using B-splines. In *Proc. 9th Int. Conference on Medical Image Computing and Computer-Assisted Intervention - Part II*, pages 702–709. Springer, 2006.

J.H. Song, G.E. Christensen, J.A. Hawley, Y.W., and J.G. Kuhl. Evaluating image registration using nirep. In *Proc. 4th Int. Workshop on Biomedical Image Registration*, pages 140–150. Springer, 2010.

T. Vercauteren, X. Pennec, A. Perchant, and N. Ayache. Symmetric log-domain diffeomorphic registration: A demons-based approach. In *Proc. 11th Int. Conference on Medical Image Computing and Computer-Assisted Intervention*, pages 754–761. Springer, 2008.

T. Vercauteren, X. Pennec, A. Perchant, and N. Ayache. Diffeomorphic demons: Efficient non-parametric image registration. *NeuroImage*, 45(1, Supp.1):61–72, 2009.

D. Yang, H. Li, D.A. Low, J.O. Deasy, and I. El Naqa. A fast inverse consistent deformable image registration method based on symmetric optical flow computation. *Physics in Medicine and Biology*, 53:6143–6165, 2008.

Z. Zhang, Y. Jiang, and H. Tsui. Consistent multi-modal non-rigid registration based on a variational approach. *Pattern Recognition Letters*, 27:715–725, 2006.